SAND2020-4657C

Proceedings of 2020 28th International Conference on Nuclear Engineering
Joint With the ASME 2020 Power Conference
ICONE28-POWER2020
August 2-6, 2020, Anaheim, CA, USA

ICONE28-POWER2020-16598

THERMAL-HYDRAULIC INVESTIGATIONS OF A HORIZONTAL DRY CASK SIMULATOR

Ramon J.M. Pulido[1], Eric R. Lindgren[1], Samuel G. Durbin[1], Alex Salazar[1]

[1]Sandia National Laboratories, Albuquerque, NM

ABSTRACT

Recent advances in horizontal cask designs for commercial spent nuclear fuel have significantly increased maximum thermal loading. This is due in part to greater efficiency in internal conduction pathways. Carefully measured data sets generated from testing of full-sized casks or smaller cask analogs are widely recognized as vital for validating thermal-hydraulic models of these storage cask designs. While several testing programs have been previously conducted, these earlier validation studies did not integrate all the physics or components important in a modern, horizontal dry cask system.

The purpose of this investigation is to produce data sets that can be used to benchmark the codes and best practices presently used to calculate cladding temperatures and induced cooling air flows in modern, horizontal dry storage systems. The horizontal dry cask simulator (HDCS) has been designed to generate this benchmark data and complement the existing knowledge base.

Transverse and axial temperature profiles along with induced-cooling air flow are measured using various backfills of gases for a wide range of decay powers and canister pressures. The data from the HDCS tests will be used to host a blind model validation effort.

Keywords: spent nuclear fuel, horizontal dry storage cask, model validation

NOMENCLATURE

BWR	boiling water reactor
BR	blockage ratio
CFD	computational fluid dynamics
CIEMAT	Centro de Investigaciones Energéticas, MedioAmbientales y Tecnológicas
CYBL	Cylindrical Boiling
DAQ	data acquisition
ENUSA	Empresa Nacional del Uranio, S.A., S.M.E.
DCS	Dry Cask Simulator
HDCS	Horizontal Dry Cask Simulator
HSM	Horizontal Storage Module
MgO	magnesium oxide
NE	nuclear energy
NRC	Nuclear Regulatory Commission
PNNL	Pacific Northwest National Laboratory
PWR	pressurized water reactor
SCR	silicon-controlled rectifier
SFWD	Spent Fuel and Waste Disposition
TC	thermocouple
UPM	Universidad Politécnica de Madrid

1. INTRODUCTION

The performance of commercial spent nuclear fuel dry storage cask systems is typically evaluated through detailed analytical modeling of the system's thermal performance. These modeling efforts are performed by the vendor to demonstrate both performance and regulatory compliance and are independently verified by the Nuclear Regulatory Commission (NRC). The majority of commercial dry storage cask systems currently in use are aboveground in both horizontal and vertical orientations. Cooling of the assemblies located inside the sealed canister is enhanced by the induced flow of air drawn in the bottom of the cask enclosure and exiting out the top of the cask enclosure.

Carefully measured data sets generated from testing of full-sized casks or smaller cask analogs are widely recognized as vital for validating design and performance models, and numerous testing studies have been previously conducted [1-4]. Recent advances in dry storage cask designs have significantly increased the maximum thermal load allowed in a canister in part by improving the efficiency of internal conduction pathways and by enhancing internal convection through greater canister helium pressure. Horizontal, canistered cask systems rely on ventilation between the canister and the vault walls to convect heat away from the canister to the surrounding environment. While several testing programs have been previously conducted, these earlier validation attempts did not incorporate new design features and

corresponding physics important in modern horizontal dry cask systems. Thus, the enhanced performance of modern horizontal dry storage systems cannot be fully validated using previous studies.

1.1 Previous Studies

Two single assembly investigations were documented in the mid-1980s [1, 3]. Both included electrically heated 15×15 pressurized water reactor (PWR) assemblies with thermocouples (TCs) installed to directly measure the surface temperature of the cladding. In Bates [1] the electrically heated assembly was instrumented with fifty-seven TCs distributed over seven axial locations. A single irradiated assembly was also studied using 105 TCs distributed equally into each of the fifteen guide tubes at seven axial locations. In Irino *et al.* [3] the electrically heated assembly was instrumented with ninety-two TCs distributed over four axial locations. All testing included horizontal orientation using helium or air at one atmosphere but imposed a constant temperature boundary condition on the outer cask wall in order to obtain prototypic storage temperatures in the fuel assembly bundle. None of these tests incorporated naturally convective cooling through induced air flow inside of vault-like enclosures.

In a recent investigation [5], an existing electrically-heated but otherwise prototypic boiling water reactor (BWR) Incoloy-clad test assembly was deployed inside of a representative storage basket and cylindrical pressure vessel that represents a vertical canister system. The symmetric single assembly geometry with well-controlled boundary conditions simplified interpretation of results. Two different arrangements of ducting were used to mimic conditions for aboveground and belowground storage configurations for vertical, dry cask systems with canisters. Transverse and axial temperature profiles were measured throughout the test assembly. The induced air mass flow rate was measured for both the aboveground and belowground configurations. In addition, the impact of cross-wind conditions on the belowground configuration was quantified.

Over 40 unique data sets were collected and analyzed for these efforts. Fourteen data sets for the aboveground configuration were recorded for powers and internal pressures ranging from 0.5 to 5.0 kW and 0.3 to 800 kPa absolute, respectively. Similarly, fourteen data sets were logged for the belowground configuration starting at ambient conditions and concluding with thermal-hydraulic steady state. Over thirteen tests were conducted using a custom-built wind machine. The results documented in the BWR dry cask simulator (DCS) test report [5] highlight a small, but representative, subset of the available data from this test series.

Data sets from the vertically oriented dry cask simulator were used in a model validation activity [6]. In this study, a model validation exercise was carried out using the data obtained from dry cask simulator testing in the vertical, aboveground configuration. Five modeling institutions – Nuclear Regulatory Commission, Pacific Northwest National Laboratory (PNNL), Centro de Investigaciones Energéticas, MedioAmbientales y Tecnológicas (CIEMAT), and Empresa Nacional del Uranio, S.A., S.M.E. (ENUSA) in collaboration with Universidad Politécnica de Madrid (UPM) – were granted access to the input parameters from the DCS Handbook, SAND2017-13058R [7], and results from the vertical aboveground BWR dry cask simulator tests reported in NUREG/CR-7250 [5]. With this information, each institution was tasked to calculate minimum, average, and maximum fuel axial temperature profiles for the fuel region as well as the axial temperature profiles of the DCS structures. Transverse temperature profiles and air mass flow rates within the dry cask simulator were also calculated. These calculations were done using modeling codes (ANSYS FLUENT, STAR-CCM+, or COBRA-SFS), each with their own unique combination of modeling assumptions and boundary conditions. For this validation study, four test cases of the vertical, aboveground dry cask simulator were considered, defined by two independent variables – either 0.5 kW or 5 kW fuel assembly decay heat, and either 100 kPa or 800 kPa internal helium pressure. However, this model validation activity was not fully blind in that all the modeling participants had access to complete data sets. Data from the present investigation using the HDCS will be used to host a blind model validation effort.

1.2 Present Test Series

The present investigation uses the same simplified, well-characterized single-assembly test apparatus [5] repositioned from a vertical to a horizontal configuration that integrates the dominant physics in prototypic horizontal systems. This approach differs from previous studies in several major respects. Principal among these is that the ventilated boundary conditions for a horizontal configuration are explicitly considered. Accurate, induced air flow rates were measured using the successful approach used in previous studies [5]. Rather than striving to achieve prototypic peak clad temperatures by artificially imposing a temperature boundary condition on the canister wall, the present study incorporates relevant physics by including realistic boundary conditions.

Additionally, the apparatus contained a hydraulically and thermally prototypic mock assembly that uses compacted magnesium oxide (MgO) powder as a spent nuclear fuel surrogate. MgO was chosen because its thermal mass was experimentally determined to be similar to uranium oxide's thermal mass [8]. The mock assembly can also accommodate elevated pressures. The pressure vessel allowed testing at prototypic pressures of 100 to 800 kPa. Testing at higher pressures was conducted in order to experimentally quantify the contribution of convection and evaluate the assumption that convective heat transfer inside the canister is negligible.

As was the case in the previous vertical DCS studies [5] a scaling distortion in simulated assembly power is necessary to more closely match the thermal-hydraulic response of a full-sized spent fuel storage cask. This need for additional decay heat is reasonable given the higher external surface-area-to-volume ratio of a single assembly arrangement as in the HDCS compared to a modern canister with up to eighty-nine assemblies. A maximum power of 5.00 kW, uniformly distributed across the single assembly, was applied to obtain peak cladding

temperatures near the maximum allowable regulatory limit of 400 °C in the system. [9]

2. MATERIALS AND METHODS

2.1 General Construction

The core of the vertical dry cask simulator used in previous studies [5] was modified for configuration to a horizontal orientation. The general design details with the required support modifications are shown in Figure 1. The quadrant labeling scheme shown in the figure follows from the orientation previously used in the vertical dry cask simulator and is meant to demonstrate how the core was transitioned from the vertical to the horizontal orientation; NUREG/CR-7250 [5] shows the original, vertical orientation. As before, an existing electrically heated but otherwise prototypic 9×9 BWR Incoloy-clad test assembly was deployed inside of a representative storage basket and cylindrical pressure vessel that represents the canister. Transverse and axial temperature profiles as well as induced cooling air flow rates have been measured for a wide range of decay power and canister pressures.

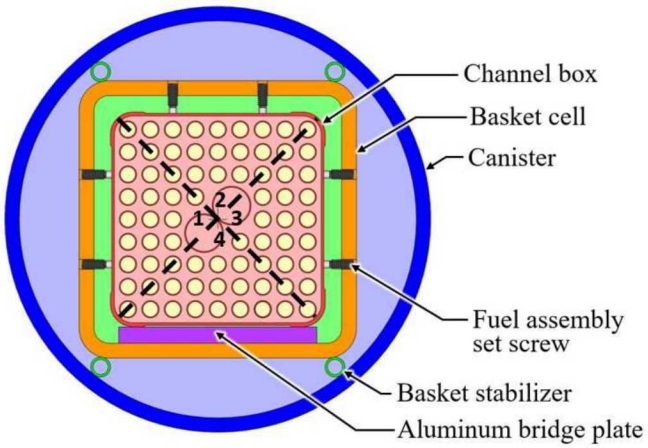

FIGURE 1: GENERAL DESIGN DETAILS OF THE DRY CASK SIMULATOR WITH HORIZONTAL CONFIGURATION MODIFICATIONS. TRIANGULAR QUADRANTS (LABELED 1-4) INDICATE THE SPATIAL ORIENTATION OF THE ASSEMBLY.

In prototypic horizontal systems, the assemblies are free to make direct contact with the bottom face of the basket. Due to existing mechanical fixturing and instrumentation at the fuel assembly base, the HDCS assembly is not free to make direct contact with the basket and must maintain concentricity to avoid damage during reorientation to a horizontal configuration. Therefore, a full-length aluminum (alloy 6061) bridge plate 127 mm (5 in.) wide and 9.6 mm (0.378 in.) thick was installed between the assembly channel box and the inside face of the basket to establish a conductive pathway and maintain concentric spacing of the assembly. Set screws were also installed through the basket on the other three sides to center and stabilize the channel box. Geometric details of the contact between the aluminum plate and the channel box are shown in Figure 2.

There is limited contact between the corners of the channel box and the aluminum bridge plate. Of the 127 mm width of the bridge plate, only a total of 13.4 mm (0.528 in.) makes direct contact with the channel box shoulders and the center 97 mm (3.82 in.) is separated by a 0.9 mm (0.0354 in.) gas gap.

Full-length stabilizing tubes along the corners of the basket provided limited conductive paths between the basket and the pressure vessel while keeping the basket centered in the pressure vessel and limiting convective cells as shown in Figure 1 and Figure 3. The stainless steel 304 tubes had an outer diameter of 12.7 mm (0.500 in.) and wall thickness of 1.59 mm (0.0625 in.). The tubes were stitch welded to the basket at 0.61 m (24 in.) intervals from the basket bottom to the top. These stitch welds had a nominal length of 25.4 mm (1.00 in.). Once the pressure vessel was installed, these stabilizer tubes formed line contacts on both the basket and the pressure vessel.

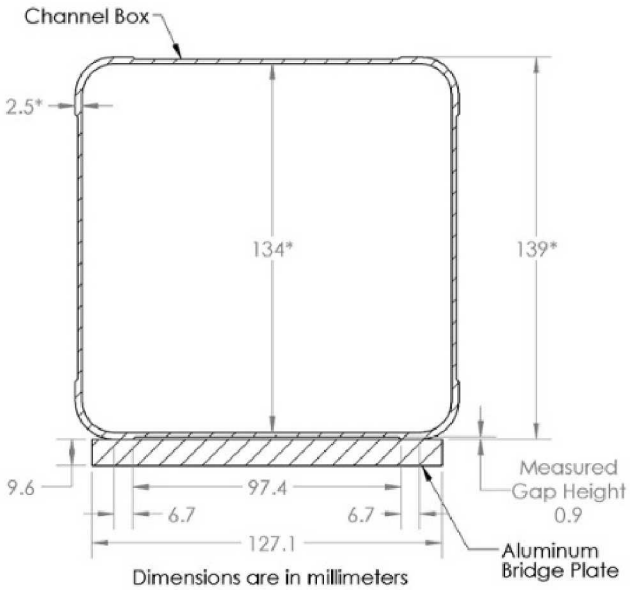

FIGURE 2: CHANNEL BOX AND ALUMINUM BRIDGE PLATE DIMENSIONS, INCLUDING THE CONTACT DIMENSIONS AND THE DIMENSIONS OF THE GAP BETWEEN THE CHANNEL BOX AND BRIDGE. DIMENSIONS MARKED BY AN ASTERISK ARE FROM YAMAMOTO *ET AL.* [10]

FIGURE 3: PHOTOGRAPHS OF THE TEST ASSEMBLY SHOWING THE BASKET STABILIZER RODS.

The horizontal test apparatus is enclosed in a stainless-steel sheet metal enclosure, backed with 6.4 mm (0.25 in.) of high-temperature, alumina-silica insulation, that simulates the concrete vault as shown in the partially exploded view in Figure 4. The vault is comprised of 11-gauge stainless steel sheet metal components. Three side ribs on each side support two side panels and two top panels. Panels on each end enclose around the pressure vessel pipe. Inlet and outlet vents to the vault enclosure are located on the top and bottom of each of the four side panels. The vault inlets are supplied by rectangular ducts in which the induced flow is measured using hot wire anemometers. Because the induced flow for the HDCS is expected to be similar to that measured in the aboveground vertical DCS study, the inlet ducts are designed to be the same size. The flow area of the vault inlet and outlet vents also match the flow area of the inlet ducts. The exterior of the sheet metal is covered with a thin layer of insulation to mimic the thermal resistance of the walls in a commercial concrete vault.

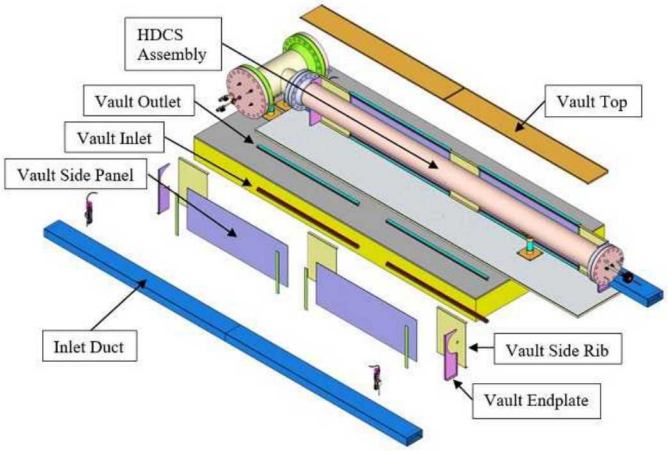

FIGURE 4: HDCS AND PARTIALLY EXPLODED SHEET METAL COMPONENTS.

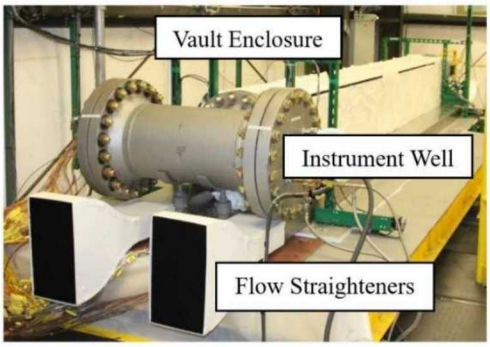

FIGURE 5: HORIZONTAL DRY CASK SIMULATOR TEST APPARATUS WITH THE INSULATED VAULT ENCLOSURE, THE INSTRUMENT WELL, AND THE AIR FLOW STRAIGHTENERS.

A photograph of the HDCS assembly is shown in Figure 5. The assembly is comprised of the electrically-heated DCS fuel assembly, the outer structures (channel box, basket, and pressure vessel representing the storage cask), and the insulated stainless-steel metal enclosure that simulates a commercial concrete vault. Also visible in the photo is the instrument well, where instrumentation for measuring temperatures and pressures are located, and the air flow straighteners.

The new test configuration was assembled and operated inside of the Cylindrical Boiling (CYBL) test facility, which is the same facility used for earlier studies [5, 8]. The apparatus was lifted out of the CYBL vessel and rotated to a horizontal orientation on a platform on the third (top) floor of the CYBL building. Figure 6 shows a scaled diagram of CYBL facility with the DCS inside. The stainless-steel vault enclosure has been assembled around the pressure vessel after it is laid in the horizontal position.

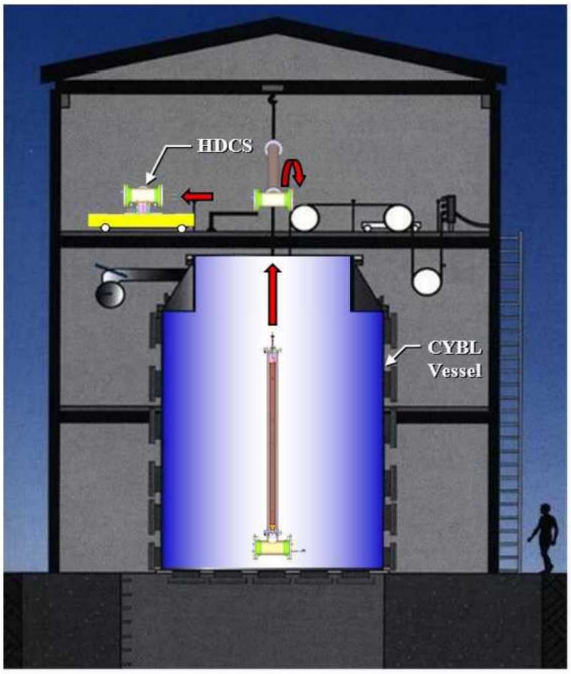

FIGURE 6: CYBL FACILITY HOUSING DRY CASK SIMULATOR TESTING.

The HDCS enclosure was scaled to a NUHOMS Horizontal Storage Module (HSM) Model 80 and Model 102 vault containing a NUHOMS 61BT canister by the blockage ratio (BR) defined as the ratio of the diameter of the canister to the inside width of the vault as shown in Figure 7. For design purposes, the air mass flow rate for the HDCS was assumed from values measured during similar, vertical test conditions [5]. This assumption was justified by observing the comparability in the air mass flow calculated by the modeling two prototypic systems NUHOMS HSM (0.25 kg/s) and the Holtec HI-STORM 100 (0.32 kg/s) with computational fluid dynamics (CFD) [11]. Thus, the inlet and outlets to the vault enclosure were designed to have a flow area that matched the aboveground, vertical DCS apparatus. As with the aboveground vertical case, the HDCS has four inlet ducts each with inside dimensions of 0.102 m (4.02 in.) by 0.229 m (9.02 in.). Air velocity anemometers were used to measure the inlet flow rate. Computer-controlled stages were

used to have the anemometers automatically traverse across the inlet opening to measure the cross-section velocity field.

A simple analysis using one-dimensional thermal resistances for combined heat transfer was performed for the vault side walls and top of an HSM and the HDCS. This analysis showed that the combined thermal resistance of the HSM vault from the heat shield to the outside of the concrete wall was equivalent to the stainless steel HDCS vault wall backed with 6.4 mm (0.25 in.) of high-temperature, alumina-silica insulation. Thus, the analysis includes the effects of the heat shield from radiation and convection. The equivalency of a relatively thin layer of insulation to 0.51 m (20 in.) of reinforced concrete with a heat shield may be realized in large part because the thermal conductivity of the insulation is roughly 30 times less than that of the concrete. Therefore, the two systems will lose thermal energy through the vault walls at the same rate for the same temperature on the HSM heat shield as on the HDCS vault interior wall. More details on the dimensional analysis relating the HDCS to the commercial HSM are described elsewhere [12].

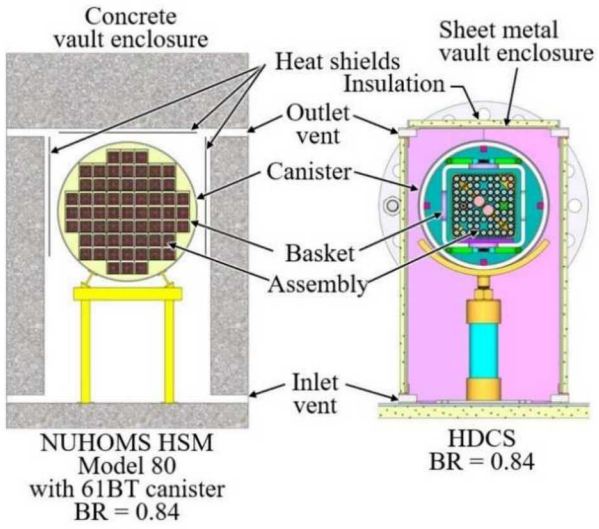

FIGURE 7: CROSS SECTIONS OF A NUHOMS HSM MODEL 80 AND THE HORIZONTAL DRY CASK SIMULATOR.

2.2 Heated Fuel Bundle Details

The highly prototypic fuel assembly was modeled after a 9×9 BWR. Commercial components were purchased to create the assembly including the top and bottom tie plates, spacers, water rods, channel box, and all related assembly hardware (see Figure 8).

Incoloy heater rods were substituted for the fuel rod pins for heated testing. Due to fabrication constraints the diameter of the Incoloy heaters was slightly smaller than prototypic rods, 10.9 mm (0.430 in.) versus 11.2 mm (0.440 in.). The slightly simplified Incoloy mock fuel rods were fabricated based on drawings and physical examples from the nuclear component supplier. The dimensions of the assembly components are provided in Table 1. Note that the number of heater rods (pins) changes from 74 to 66 between the lower and upper sections, due to 8 partial-length rods that run 2.61 m from the top of the bottom tie plate. The assembly was hydraulically characterized in a previous study [8].

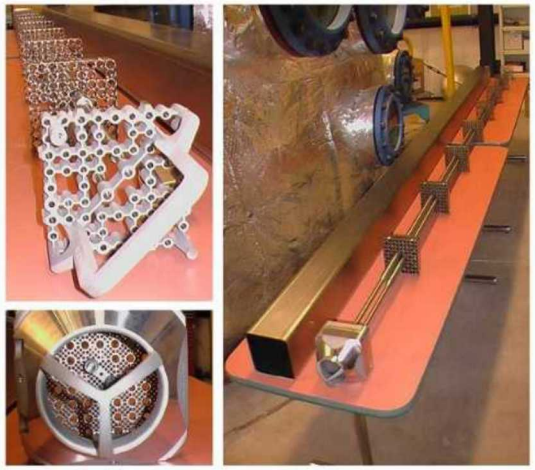

FIGURE 8: 9×9 BWR COMPONENTS USED TO CONSTRUCT THE TEST ASSEMBLY INCLUDING TOP TIE PLATE (UPPER LEFT), BOTTOM TIE PLATE (BOTTOM LEFT) AND CHANNEL BOX AND SPACERS ASSEMBLED ONTO THE WATER RODS (RIGHT).

Description	Lower (Full) Section	Upper (Partial) Section
Number of pins	74	66
Full heater rod length (m)	3.96	
Partial heater rod length (m)	2.61	
Heater OD (mm)	10.9	
Pin pitch (mm)*	14.4	
Pin separation (mm)	3.48	
Water rod OD (main section) (mm)*	24.9	
Water rod ID (mm)*	23.4	
Channel box length (m)	4.13	
Channel box ID (mm)*	134	
Channel box OD (mm)*	139	
Corner channel box wall (mm)*	2.5	

*Yamamoto *et al.* [10]

TABLE 1: DIMENSIONS OF ASSEMBLY COMPONENTS IN THE MOCK 9×9 BWR.

2.3 Pressure Control

Two high-accuracy 0 to 1,034 kPa (0 to 150 psia) absolute pressure transducers (Setra Systems ASM1-150P-A-1M-2C-03-A-01) are installed in the instrument well (see Figure 5). The pressure measurements are made in duplicate due to the importance of the measurement. The experimental uncertainty associated with these gauges is ±0.05% of full scale, or ±0.52 kPa (±0.075 psi).

All penetrations and fittings were selected for the apparatus to have helium leak rates of 1×10^{-6} std. cm^3/s or better at 100 kPa. In addition, spiral-wound gaskets capable of leak rates of

better than 1×10^{-7} std. cm^3/s were used to form the seals at each flange. The ANSI N14.5 leak rate of 1×10^{-4} std. cm^3/s [13] would result in an observable pressure drop of 0.03 kPa (4×10^{-3} psi) after a one-week period, which is far below the experimental uncertainty of 0.52 kPa (0.075 psi). During previous testing, leaks in the as-built apparatus were identified and repaired as best as possible [5]. Ultimately, a small leak path of undetermined origin remains, and a positive pressure control system was implemented to maintain pressure.

This pressure control system used the high-accuracy, absolute-pressure transducers, three low-flow needle valves, and three positive-shutoff actuator valves under control of the LabView data acquisition (DAQ) system (see Figure 9). Two actuator valves (vent) control flow out of the vessel, and the third valve (fill) controls the fill gas flow into the vessel. As the vessel heats up, the expanding backfill gas vents out of the first actuator and needle valve to maintain a constant pressure. A second vent valve (overflow) activates if the vessel continues to pressurize. As steady state is reached, the small leak will slowly reduce the backfill pressure, at which point the control system opens the third actuator valve (fill) to allow a small flow through the third needle valve. Overall, a similar pressure control system used in past testing was able to maintain the vessel pressure constant to within ±0.3 kPa (0.044 psi).

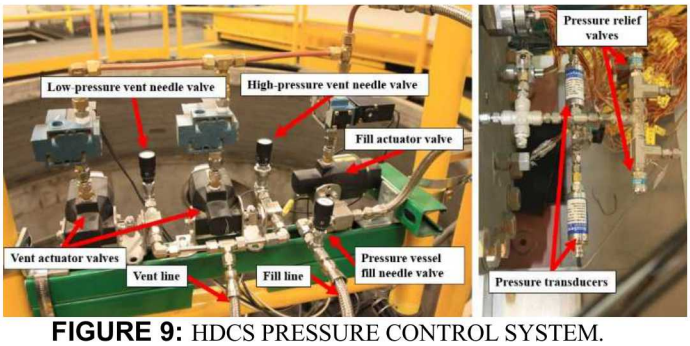

FIGURE 9: HDCS PRESSURE CONTROL SYSTEM.

The pressure vessel internal volume was measured during previous testing [5]. The total internal volume was determined to be 252.0 liters, with an uncertainty of ±2.6 liters. This measurement includes the volume of the instrument well that is insulated from the heated test section.

2.4 Power Control

The electrical voltage and current delivered to the test assembly heaters is controlled to maintain a constant power by a digital silicon-controlled rectifier (SCR). The DAQ system provides a power setpoint to the SCR that is constantly compared to the measured output power. The power, voltage, and current measurements are collected by the DAQ. A special calibration schedule of thirty-two points was ordered for the power diagnostic (Ohio Semitronics PTB-112D1PCY48). The observed 95% uncertainty based of the Student's t-value and the standard error of the regression for this instrument give an uncertainty of U_{Watt} = ±13 W. Additional details on the power control system and the instrumentation panel may be found in the full test documentation [12].

2.5 Temperature Measurements

Ninety-two TCs were previously installed on the BWR test assembly, and 106 TCs were installed on the vault enclosure and the external ambient temperature regions. The TCs used are ungrounded junction type-K with an Incoloy sheath diameter of 0.762 mm (0.030 in.). Within the test assembly, these are held in intimate contact with the cladding by a thin Nichrome shim. This shim is spot welded to the cladding, as shown in Figure 10. The TC attachment method allows the direct measurement of the cladding temperature.

FIGURE 10: TC ATTACHMENT TO HEATER ROD.

Additional TCs were installed on the other major components of the test apparatus such as the channel box, storage basket, canister wall, and exterior air ducting, as well as on the vault enclosure. TCs were also suspended in air surrounding the test apparatus to measure ambient temperatures. TC placement on these components was designed to align with the existing TC placement in the BWR assembly. Based on the need to optimally balance the TC routing through the assembly, the axial and transverse arrays of TCs were distributed among three of four triangular quadrants (see Figure 1) relying on the assumption of axial symmetry that was valid for the initial, vertical orientation studied previously. However, the assumption of axial symmetry is not valid in the horizontal orientation. Details of these TC locations, including the various axial locations and the orientation of the quadrants in which the TCs were placed, are described in previous testing documentation [5, 8, 12].

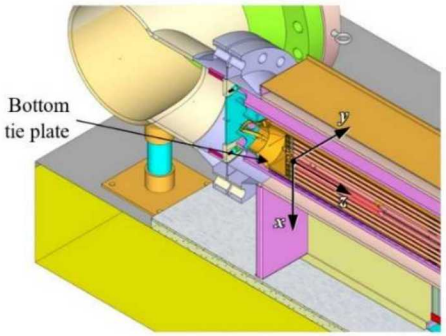

FIGURE 11: DEFINITION OF COORDINATE REFERENCES IN THE TEST APPARATUS.

Error! Reference source not found. shows the definition of the reference coordinate system. The reference origin is defined as the center of the top surface of the bottom tie plate. Based on the previous vertical orientation of the test apparatus inside of the CYBL vessel, the assembly was laid on the aluminum bridge plate on the quadrant, which lacks any TCs in the tube bundle (quadrant 4).

2.6 Air Flow Measurements

Figure 12 shows the air flow pattern through the HDCS vault. Cold air is drawn into the air inlet ducts and flows into the vault inlets on the sides of the enclosure. The air is heated as it passes between the vault and the simulated canister. The hot air exhausts at the top of the enclosure sides via the vault outlets. The hot wires are mounted on motorized stages (Velmex Stage XN10-0040-M02-71, Motor PK245-01AA). The data acquisition computer communicated with the stage controller (Velmex Controller VXM-4) to identify and verify hot wire positioning.

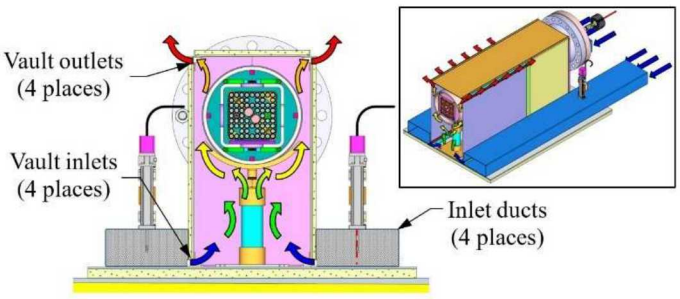

FIGURE 12: AIR FLOW PATTERN IN THE HDCS FROM NATURAL CONVECTION.

The methods for determining the induced air flow in the HDCS used hot wire anemometers to measure inlet air velocity and subsequently calculate an overall air mass flow rate. The hot wire anemometers used are TSI model 8455 – the tip detail is shown in Figure 13. For scale, the largest shaft diameter shown is 6 mm (0.25 in.). The sensing element of the model 8455 is protected inside of an open cage and is sensitive to flows down to 0.13 m/s (25 ft/min) with a response time of 0.2 seconds. Details of the hot wire anemometer placements and calculations of the air mass flow rates based on the anemometer measurements can be found elsewhere [12].

FIGURE 13: PHOTOGRAPH OF THE HOT WIRE ANEMOMETER TIP.

To obtain the most stable and repeatable measurements possible, a honeycomb element is inserted into all four assembly inlets to align the flow in the desired direction and reduce any turbulence on the hot wire anemometers. A polycarbonate honeycomb element was chosen with a cell diameter, wall thickness, and flow length of 3.8, 0.1, and 25.8 mm (0.150, 0.004, and 1.015 in.), respectively. This type of flow straightening element has been found to provide the greatest reduction in hot wire fluctuations while introducing the smallest pressure drop to the system. The effective, frictional coefficient for this honeycomb material was found to be $D = 1.35\times10^{6}$ m^{-2} for porous media in CFD simulations.

The flow straightener section featured a convergent nozzle made of corrugated fiberboard and scrim-backed, pressure-sensitive tape to minimize the flow losses associated with the honeycomb element by increasing the flow area by a factor of four. The honeycomb dimensions used in each of the four inlets was 0.425 m (16.7 in.) tall by 0.233 m (9.2 in.) wide and 0.0258 m (1.02 in.) thick for a flow area of 0.099 m^2. The nozzle design included two straight sections to accommodate the honeycomb and the assembly inlet. Long-sweep arcs with matching tangents at the inflection point were chosen to provide a smooth transition from the honeycomb section to the assembly inlet.

2.7 HDCS Test Matrix

The HDCS test series is comprised of ten test runs as summarized in Table 2. Both helium and air were used as fill gases. The fill pressure was either 100 kPa or 800 kPa for helium. For air, the fill pressure was 100 kPa. For air and helium at 100 kPa the assembly was powered at four power levels: 0.50, 1.00, 2.50, and 5.00 kW. For helium at 800 kPa the assembly was powered at either 0.50 or 5.00 kW. The power was uniformly distributed across the assembly, along the heated lengths.

To facilitate a blind modeling validation exercise, data for the comparison metrics listed in Table 3 have been provided for two of the test runs for model calibration [12] – a summary of the data is included in this paper. Modeling validation participants will be asked to provide the same information calculated for all of the runs listed in Table 2.

Fill Gas	Pressure (kPa)	Power (kW)
Helium	100	0.50
	100	1.00
	100	2.50
	100	5.00
	800	0.50
	800	5.00
Air	100	0.50
	100	1.00
	100	2.50
	100	5.00

TABLE 2: HDCS TEST MATRIX. TESTS WITH RESULTS PRESENTED IN THIS PAPER ARE RUNS HIGHLIGHTED IN GREY.

Metric	Notes
Peak Cladding Temperature	PCT
PCT - Location	x, y, z
Air mass flow rate	$\dot{m}_{Air}$
Axial temperature profile	T(z) at assembly center (5 locations)
Transverse x-axis temp. profile	T(x) at z = 48 in. (11 locations)
Transverse y-axis temp. profile	T(y) at z = 72 in. (7 locations)

TABLE 3: PROPOSED STEADY-STATE COMPARISON METRICS.

3. RESULTS AND DISCUSSION

The criterion for steady state was considered met when the first derivative with respect to time of the temperatures in the test apparatus was ≤ 0.3 K/h. The steady state values reported here represent the average of data collected from the point this criterion was met in the majority of data channels to the end of the test.

Table 4 shows the steady-state results for the 2.50 kW, 100 kPa case with helium as the fill gas. The table lists the average, maximum, and minimum values for the applied power, peak temperatures of the cladding, peak ambient temperatures, and the total induced cooling air flow rate. More temperatures for the components outside of the fuel assembly are provided elsewhere [12]. Table 5 shows the same steady-state results for the 2.50 kW, 100 kPa case with air as the fill gas. The power for the two tests was essentially the same and stable at 2.50 kW. The induced air flow in the helium fill test was slightly higher than in the air-filled test but within experimental error, $U_{\dot{m},\,Total} = \pm 3\times10^{-4}$ kg/s.

	Power (kW)	PCT (K)	Ambient (K)	Tot. Flow Rate (kg/s)
Average	**2.503**	**558.7**	**296.7**	**0.0283**
Max	2.515	559.4	302.3	0.0286
Min	2.493	557.9	294.0	0.0273
z-Location (m)		1.22		

TABLE 4: STEADY-STATE PEAK TEMPERATURE, AMBIENT TEMPERATURE, AND AIR MASS FLOW RATE RESULTS IN THE 2.50 kW 100 kPa CASE WITH HELIUM.

	Power (kW)	PCT (K)	Ambient (K)	Tot. Flow Rate (kg/s)
Average	**2.500**	**647**	**297**	**0.0277**
Max	2.519	647	301	0.0280
Min	2.484	647	295	0.0268
z-Location (m)		0.61		

TABLE 5: STEADY-STATE PEAK TEMPERATURE, AMBIENT TEMPERATURE, AND AIR MASS FLOW RATE RESULTS IN THE 2.50 kW 100 kPa CASE WITH AIR.

The steady-state internal fuel bundle axial temperature profiles for the 2.50 kW, 100 kPa test cases with fills of helium and air are shown in Figure 14 and Figure 15, respectively. The location of the thermocouples used to produce the profile is indicated on the inset of the fuel bundle cross-section. Most of the TCs are attached to fuel rods at the locations indicated by the blue diamonds and green triangles. A few TCs are located on the water rods (red squares). The peak cladding temperature is located at the star symbol.

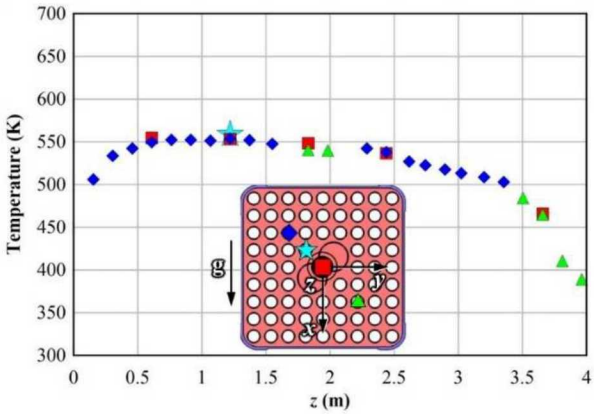

FIGURE 14: INTERNAL TEMPERATURE PROFILE AS A FUNCTION OF z FOR 2.50 kW AND HELIUM AT 100 kPa. THE DIRECTION OF GRAVITY IS INDICATED BY "g".

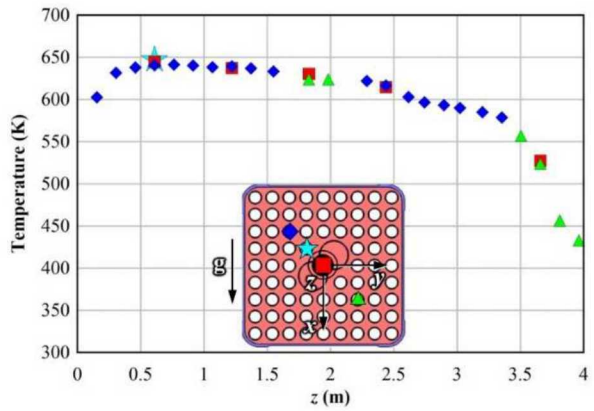

FIGURE 15: INTERNAL TEMPERATURE PROFILE AS A FUNCTION OF z FOR 2.50 kW AND AIR AT 100 kPa. THE DIRECTION OF GRAVITY IS INDICATED BY "g".

The temperatures in the fuel bundle were all lower with the helium backfill than with the air backfill. The shapes of the axial profiles are similar although the profile is flatter in the lower fully populated bundle in the helium fill case. For both cases the temperature profile drops more steeply with increased axial location after the partial rods end in the bundle at z = 2.6 m and again at the end of the heated zone at z = 3.7 m.

The steady-state vertical temperature profiles for the 2.50 kW, 100 kPa fill of helium and air are shown graphically in Figure 16 and Figure 17, respectively. The scaled inset figure on the right shows the location of the thermocouples. The profile

passes through the center line of the apparatus along the x-axis at $z = 1.219$ m. TCs are located on the top and bottom of the vault enclosure, pressure vessel, storage basket and channel box. TCs are also located inside the assembly on the water rods and heater rods. The TCs providing data points in Figure 16 and Figure 17 are located at the center and above the center of the assembly.

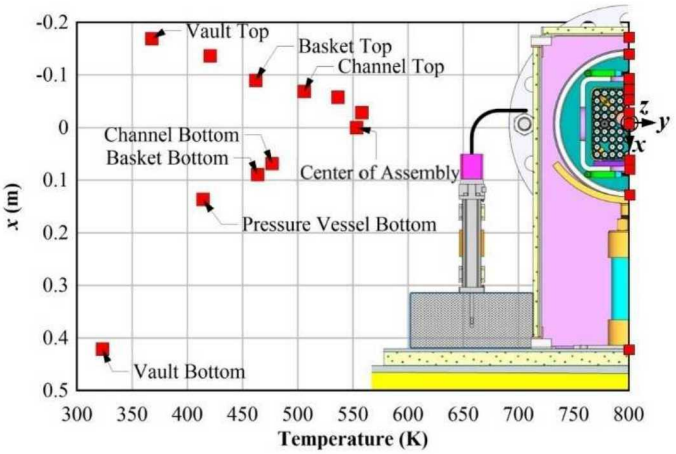

FIGURE 16: VERTICAL TEMPERATURE PROFILE FOR 2.50 kW, $z = 1.219$ m (48.0 in), AND HELIUM AT 100 kPa.

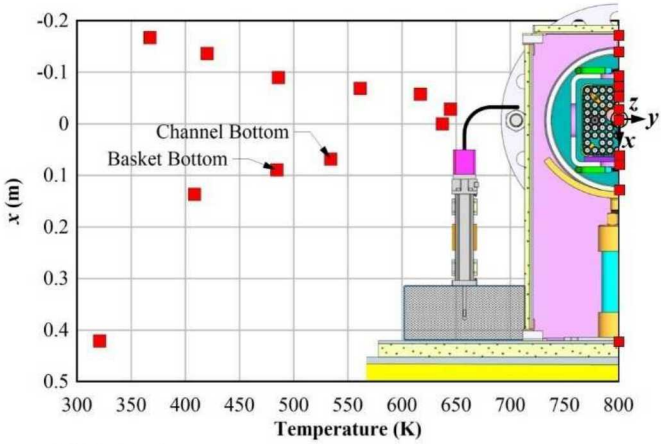

FIGURE 17: VERTICAL TEMPERATURE PROFILE FOR 2.50 kW, $z = 1.219$ m (48.0 in), AND AIR AT 100 kPa.

The peak temperature for both cases was located above the center of the assembly, but the peak temperature for the helium fill case was 87 K cooler than the air fill case. For the air case the temperature of the bottom of the storage basket was 1.5 K lower than the top of the storage basket. For the helium case the situation is reversed and the temperature of the bottom of the storage basket was 1.5 K higher than the top of the storage basket. This temperature difference is within the experimental error of the temperature measurement. More significant is the temperature difference between the bottom of the storage basket and the bottom of the channel box. For the air case this temperature difference is 50 K. For the helium case the temperature difference between the channel and the basket is reduced to 13 K indicating much better thermal coupling by the aluminum bridge plate when the gap between the bridge plate and the channel box (see Figure 2) is filled with helium. The temperature difference between the basket and the pressure vessel is also less in the helium case.

The steady-state horizontal temperature data for the 2.50 kW, 100 kPa fill of helium and air are shown in Figure 18 and Figure 19, respectively. The unscaled inset figure in the bottom left shows the location of the thermocouples. The profile passes through the center line of the apparatus along the y-axis at $z = 1.829$ m. The profile starts in the center of the assembly and proceeds out in the positive y-direction. The TCs shown in the plot are located at the center of the fuel assembly, at fuel rods adjacent to the center of the assembly, the channel box, the basket, the pressure vessel, and the vault wall.

The peak temperature for both cases was located just above the water rods, but the peak temperature for the helium fill case was 84 K cooler than the air fill case. As was the case in the vertical temperature profile, the temperature gradients between the components inside the pressure vessel are lower in the helium case than in the air case.

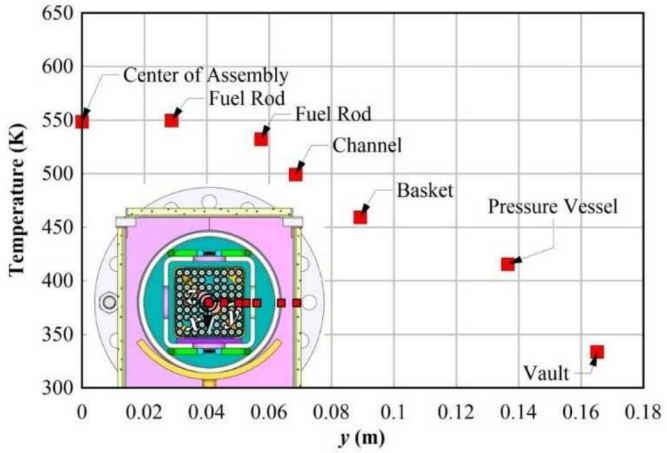

FIGURE 18: HORIZONTAL TEMPERATURE PROFILE FOR 2.50 kW, $z = 1.829$ m (72.0 in), AND HELIUM AT 100 kPa.

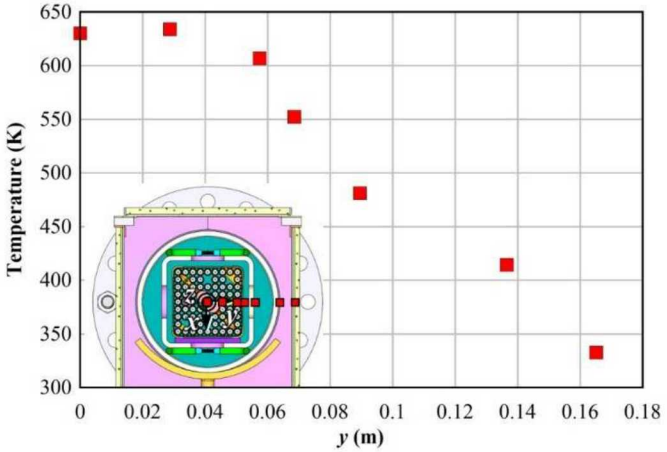

FIGURE 19: HORIZONTAL TEMPERATURE PROFILE FOR 2.50 kW, $z = 1.829$ m (72.0 in), AND AIR AT 100 kPa.

4. CONCLUSION

The purpose of the present investigation is to produce data sets that can be used to benchmark the codes and best practices presently used to determine cladding temperatures and induced cooling air flows in modern horizontal dry cask storage systems. The horizontal dry cask simulator (HDCS) has been designed to generate this benchmark data and add to the existing knowledge base. Transverse and axial temperature profiles along with induced cooling air flow are measured for a wide range of decay powers and representative (and higher) canister pressures using backfills of helium or air. Data from the HDCS tests will be used in a blind model validation study that will involve the comparison of experimental and modeling temperature profiles and air mass flow rates over a wide range of test powers and pressures.

ACKNOWLEDGEMENTS

This work was sponsored under the Department of Energy's (DOE) Office of Nuclear Energy (NE) Spent Fuel and Waste Disposition (SFWD) campaign.

The authors would like to acknowledge the hard work and commitment of all contributors to the project. In particular, we would like to acknowledge the strong support and leadership of Ned Larson at the Department of Energy. Sylvia Saltzstein and Geoff Freeze are to be commended for their programmatic and technical guidance.

The authors would also like to thank Greg Koenig, William Chavez, Adrian Perales, Kyle Tsosie, and Dominic Fascitelli for their tireless efforts and dedication to service, which made the success of this project possible.

This paper is Sandia publication SAND2020-xxxx.

REFERENCES

[1] Bates, J.M., 1986, "Single PWR Spent Fuel Assembly Heat Transfer Data for Computer Code Evaluations," PNL-5571, Pacific Northwest Laboratory, Richland, WA.

[2] Dziadosz, D., Moore, E.V., Creer, J.M., McCann, R.A., McKinnon, M.A., Tanner, J.E., Gilbert, E.R., Goodman, R.L., Schoonen, D.H., Jensen, M., and Mullen, C., 1986, "The Castor-V/21 PWR Spent-Fuel Storage Cask: Testing and Analyses," EPRI NP-4887, Project 2406-4, PNL-5917, UC-85, Electric Power Research Institute, Palo Alto, CA.

[3] Irino, M., Oohashi, M., Irie, T., and Nishikawa, T., 1987, "Study on Surface Temperatures of Fuel Pins in Spent Fuel Dry Shipping/Storage Casks," IAEA-SM-286/139P, Proceedings of Packaging and Transportation of Radioactive Materials (PATRAM '86), Volume 2, p. 585, International Atomic Energy Agency, Vienna, Austria.

[4] McKinnon, M.A., Doman, J.W., Tanner, J.E., Guenther, R.J., Creer, J.M., and King, C.E., 1986 "BWR Spent Fuel Storage Cask Performance Test, Volume 1, Cask Handling Experience and Decay Heat, Heat Transfer, and Shielding Data," PNL-5777 Vol. 1, Pacific Northwest Laboratory, Richland, WA.

[5] Durbin, S.G. and Lindgren, E.R., 2018, "Thermal-Hydraulic Experiments Using a Dry Cask Simulator," NUREG/CR-7250, Nuclear Regulatory Commission, Washington, D.C.

[6] Pulido, R.J.M., Lindgren, E.R., Durbin, S.G., Zigh, A., Solis, J., Suffield, S.R., Richmond, D.J., Fort, J.A., Herranz, L.E., Feria, F., Penalva, J., LLoret, M., Galbán, M., Benavides, J., and Jiménez, G., 2020, "Modeling Validation Exercises Using the Dry Cask Simulator," SAND20196079R, Sandia National Laboratories, Albuquerque, NM.

[7] Lindgren, E.R. and S.G. Durbin, 2017, "Materials and Dimensional Reference Handbook for the Boiling Water Reactor Dry Cask Simulator," SAND2017-13058R, Sandia National Laboratories, Albuquerque, NM.

[8] Lindgren, E.R. and Durbin, S.G., 2013, "Characterization of Thermal-Hydraulic and Ignition Phenomena in Prototypic, Full-Length Boiling Water Reactor Spent Fuel Pool Assemblies After a Postulated Complete Loss-of-Coolant Accident," NUREG/CR-7143, SAND2007-2270, Nuclear Regulatory Commission, Washington, D.C.

[9] U.S. Nuclear Regulatory Commission, Interim Staff Guidance-11, Revision 3, "Cladding Considerations for the Transportation and Storage of Spent Nuclear Fuel," NRC Spent Fuel Project Office, November 2003.

[10] Yamamoto, A., Ikehara, T., and Ito, T., 2002, "Benchmark Problem Suite for Reactor Physics Study of LWR Next Generation Fuels," J. Nucl. Sci. Tech., 39 (8), 900-912.

[11] Solis, J. and Zigh, A., 2015, "Impact of Variation in Environmental Conditions on the Thermal Performance of Dry Storage Casks," NUREG-2174, Nuclear Regulatory Commission, Washington, D.C.

[12] Lindgren, E.R., Durbin, S.G., Pulido, R.J.M., and Salazar, A., 2019, "Update on the Thermal Hydraulic Investigations of a Horizontal Dry Cask Simulator," SAND2019-11688 R, Sandia National Laboratories, Albuquerque, NM.

[13] American National Standards Institute, 2014, "American National Standard for Radioactive Materials – Leakage Tests on Packages for Shipment," ANSI N14.5-2014, New York, NY.